KfK 2839
Dezember 1979

# Nuclear Density Distributions of $^{40,42,44,48}$Ca from Elastic Scattering of 104 MeV Alpha Particles

H. J. Gils, E. Friedman, Z. Majka, H. Rebel
Institut für Angewandte Kernphysik

Kernforschungszentrum Karlsruhe

KERNFORSCHUNGSZENTRUM KARLSRUHE

Institut für Angewandte Kernphysik

KfK 2839

# Nuclear Density Distributions of $^{40,42,44,48}Ca$ from Elastic Scattering of 104 MeV Alpha Particles

H.J. Gils, E. Friedman*, Z. Majka**, and H. Rebel

* The Racah Institute of Physics, The Hebrew University of Jerusalem, Jerusalem, Israel

** Institute of Physics, Jagellonian University, Cracow, Poland

Kernforschungszentrum Karlsruhe GmbH, Karlsruhe

Kernforschungszentrum Karlsruhe GmbH
ISSN 0303-4003

ABSTRACT

The elastic scattering of 104 MeV α particles from $^{40,42,44,48}Ca$ has been analyzed by a single folding model with a density dependent effective interaction. Nuclear density distributions have been extracted using various descriptions including Fourier-Bessel series which distinctly reduces the model dependence of the results and enables realistic estimates of errors. Differences of the density shapes of the Ca-isotopes are well determined showing evidence for a neutron skin in $^{48}Ca$. The resulting root mean square radii are compared to the results obtained from other methods. The sensitivity and limitations of various methods are discussed.

Dichteverteilungen der Atomkerne von $^{40,42,44,48}Ca$ aus elastischer Streuung von 104 MeV α-Teilchen

ZUSAMMENFASSUNG

Die elastische Streuung von 104 MeV α-Teilchen an $^{40,42,44,48}Ca$ wurde mit einem Faltungsmodell mit dichteabhängiger effektiver α-Kern-Wechselwirkung analysiert. Unter Verwendung verschiedener Verteilungsformen einschließlich der Fourier-Bessel-Methode wurde die Dichteverteilung der Kernmaterie extrahiert. Bei der Fourier-Bessel-Methode ist die Modellabhängigkeit der Ergebnisse stark reduziert. Darüberhinaus erlaubt diese Methode eine realistische Fehlerabschätzung. Die Differenzen des Dichteverlaufs werden durch die Analysen gut bestimmt und zeigen im Falle von $^{48}Ca$ die Evidenz einer Neutronenhaut. Die resultierenden mittleren quadratischen Radien werden mit den Ergebnissen anderer Methoden verglichen und die Empfindlichkeit und Grenzen der verschiedenen Methoden werden diskutiert.

## 1. INTRODUCTION

The study of nuclear density distributions by strong-interacting probes has seen a remarkable progress in recent years[1] mostly because of the great improvement in the accuracy of experimental results. The interpretations of experimental results have also been improved due to the progress in understanding the reaction mechanism involved. The α particle is one of the most preferred projectiles in this field because of its well known strong absorption at the nuclear surface and because of its vanishing spin and isospin which greatly simplifies the analysis. In addition, a finite sensitivity of α particle scattering to the interior of the nucleus[2] is observed when large scattering angles are involved thus promising to probe the whole shape of the nuclear density distribution with a reasonable accuracy.

The calcium isotopes have special significance in the study of nuclear radii because $^{40}$Ca is often used for "calibration" of the projectile-target effective interaction and also because these isotopes span a wide range of neutron numbers including two doubly-closed shell nuclei $^{40,48}$Ca which are of particular interest for nuclear structure calculations.

In the present paper we report the results of analysis of elastic scattering of 104 MeV α particles using various methods, aimed at extracting information on nuclear density distributions for calcium isotopes. This paper complements another one[3], where only optical potentials are discussed without referring to nuclear densities. Most of previous analyses of experimental data on Ca-isotopes used simple functions for the potentials or for the density distributions, and that lead sometimes to unrealistically small estimates of uncertainties[4]. It should also be emphasized that using pre-chosen analytic functions may introduce into the results systematic errors which may distort the picture of relatively small isotopic effects. Therefore one particular aspect of improving the procedures of analysis should be to remove, as much as possible, any bias originating from the analytical form of the densities put into the analysis. Concerning this point the analysis of the present experimental

results in terms of nucleon density distributions is of particular interest because large angle data are included. Only in such cases one can obtain information on the nuclear interior[2] which is a condition for the bias-free determination of nuclear densities.

In order to obtain information on nuclear density distributions one must introduce (explicitly or implicitly) a reaction model which connects the phenomenological interaction potential (optical potential) with the target density distribution. Important steps in this direction have been made by the use of folding models, an approximation essentially based on the first term of a multiple scattering expansion of the real part of the optical potential. In section II a density dependent folding model is introduced which is shown to be capable of describing large angle scattering beyond the nuclear "rainbow angle" and which gives - in contrast to simpler approaches previously applied - reasonable results for the real optical potential (central depth, volume integral per nucleon pair, rms-radii). In section III the folding model is taken one step further by introducing the Fourier-Bessel (FB) expansion into the nuclear density distribution thereby strongly reducing the dependence of the results on the functional form chosen for the analyses and also enabling to obtain realistic estimates of errors. In section IV the results of the folding model are compared with those obtained from the FB optical potentials in order to test the consistency of the results and to detect possible remaining deficiencies. Finally, in section V the results are compared with those obtained by various other methods of investigating nuclear density distributions.

## 2. FOLDING MODEL

### 2.1 "Calibration" of the Effective Interaction

In the folding model approach[5] the real part of the optical potential is related to the nuclear density distribution via an effective alpha-nucleon interaction, namely

$$\mathrm{ReU}(r) = \int V_{\alpha N}\left(\left|\vec{r}'-\vec{r}\right|\right)\, \rho_m(r')\, d^3r' \qquad (1)$$

where $\rho_m(r')$ is the point-nucleon distribution of the target nucleus.

$V_{\alpha N}$ is an effective alpha-bound nucleon interaction and the simple Gaussian form

$$V_{\alpha N}(r) = - V_G \exp\left[-|\vec{r}'-\vec{r}|^2/a^2\right] \qquad (2)$$

had been successfully used[5] for data confined to the diffraction region. (In this work we limit the discussion to single-folding models. Double-folding models have also been successfully applied to the present data[6] and have been shown to be equivalent to single-folding models particularly if refinements (e.g. exchange, density dependence) are appropriately included in both approaches). Attempts to use the effective interaction (2) for the analysis of data which extend to large angles resulted in a total failure[4,7]. The FB optical potential analysis[7] indicated the need for saturation in the effective interaction which may result from a density dependence of the NN-interaction and from the exchange effects caused by the Pauli principle. The introduction of saturation effects lead indeed[4] to good agreement between calculation and experiment. The effective interaction (2) was therefore replaced by the following form

$$V_{\alpha N}(r) = -V_G \exp\left[-|\vec{r}'-\vec{r}|^2/a^2\right] \{1-\gamma\, \rho_m^{2/3}(r')\} \qquad (3)$$

where the last factor accounts for the required saturation. The three parameters of this interaction, namely $V_G$, a, and $\gamma$ were obtained from a fit to the $^{40}$Ca data using an adopted matter density distribution $\rho_m$ for this nucleus.

To construct this matter density distribution we started from the well known <u>charge</u> distribution $\rho_{ch}$ of the $^{40}$Ca nucleus. Neglecting the influence of the charge form factor of the neutrons on the total charge distribution the latter can be converted into a point-proton distribution $\rho_p$ by unfolding the charge form factor of the proton $\rho_{cp}$ via the expression

$$\rho_{ch}(\vec{r}) = \int \rho_p(\vec{r}')\, \rho_{cp}(\vec{r},\vec{r}')d\vec{r}' \qquad (4)$$

Thereby a Gaussian form was assumed for $\rho_{cp}(r)$ having an rms radius of 0.82 fm. For simplicity we used a 3-parameter Fermi form for $\rho_{ch}(r)$ and either a 3 or a 2-parameter Fermi form for $\rho_p(r)$ when solving eq. 4 iteratively.

Since neither the neutron density distribution itself nor its rms-radius are by far as well known as the charge distribution one has to make assumptions about the neutron distribution in order to determine the total matter distribution $\rho_m = \rho_p + \rho_m$. In addition, the simple unfolding procedure of the charge distribution can at best be assumed to give a more or less good approximation of the "real" proton distribution.

For these reasons we studied the dependence of the three parameters of the effective interaction ($V_G$, a, $\gamma$).

(i) on the rms-radius assumed for the neutron or total matter density distribution of $^{40}Ca$, respectively.
(ii) on the form of the matter density distribution.
Thereby, in particular the dependence of the results of the other Ca-isotopes on the "calibration" procedure of $V_{\alpha N}$ has been observed.

For the first question (i) we used a 3-parameter Fermi form for the proton distribution as derived from eq. 4 with the parameter values

$$c_p = 3.808 \text{ fm}, \quad a_p = 0.512 \text{ fm}, \quad w_p = -0.166 \text{ fm}.$$

The same form was assumed for the neutrons keeping

$$a_n = a_p, \quad w_n = w_p$$

and varying only the half-way radius $c_n$ in order to change the rms-radius of the matter density distribution. In fig. 1 the parameter values resulting from fits to the $^{40}Ca$ cross sections are displayed versus $\langle r_n^2 \rangle^{1/2}$ assumed for the neutron distribution and the corresponding values of $\langle r_m^2 \rangle^{1/2}$, respectively. The reproduction of the experimental cross sections characterized by $\chi^2/F$, the $\chi^2$-value per degree of freedom, was nearly equally good ($\chi^2/F \sim 5.0$) for the whole range of $\langle r_n^2 \rangle^{1/2}$ investigated. However, only for the region

$$3.34 \text{ fm} \leqq \langle r_n^2 \rangle^{1/2} \leqq 3.39 \text{ fm}$$

we obtained reasonable forms and integral quantities of the real optical potentials (eq. 1) which were compatible with the well known optical potential derived by "model independent" analyses[3]. This region of $\langle r_n^2 \rangle^{1/2}$ corresponds to a difference

between the neutron and proton rms-radii $\langle r_n^2 \rangle^{1/2} - \langle r_p^2 \rangle^{1/2} = \Delta r_{np}$ of -0.045 fm to + 0.005 fm. This range, which contains the results of various Hartree-Fock predictions, can be regarded as reasonable for the calibration nucleus $^{40}$Ca. Since just in this region the resulting parameter $V_G$, a, and $\gamma$ are rather constant, we conclude that the obtained parameters for the effective interaction do not strongly depend on the particular choice of $\langle r_n^2 \rangle^{1/2}$ as long as $\langle r_n^2 \rangle^{1/2}$ is inside the reasonable range accepted for $^{40}$Ca and as long as the functional form of $\rho_m$ is not drastically changed.

On the other hand attacking question (ii) the three parameters came out to be quite sensitive to the details of the <u>form</u> of the density assumed for $^{40}$Ca. For example Fig. 2 shows two different density distributions $\rho_m$ used for $^{40}$Ca. The smooth curve is the 3-parameter Fermi distribution

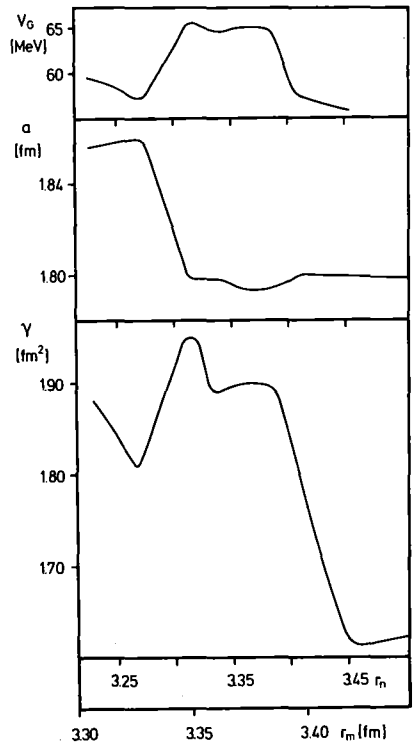


Fig. 1: Parameters of the effective interaction as determined by assuming different rms-radii for the neutron distribution of $^{40}$Ca.

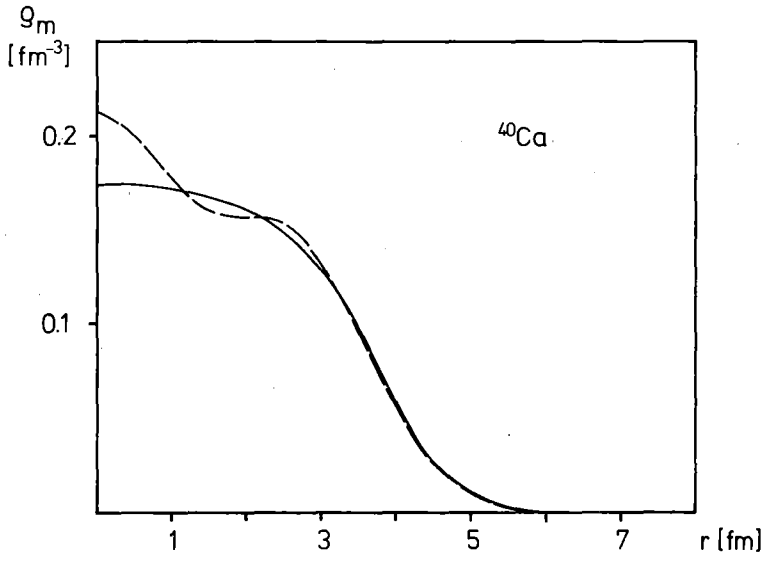


Fig. 2: Nuclear density distributions for $^{40}$Ca. Solid line: 3-parameter fermi-function derived from experimental charge distributions. Dashed line: density distribution obtained from shell model calculations (see text).

mentioned above with $\Delta r_{np} = -0.04$ fm and the dashed curve represents $\rho_m$ obtained by filling protons and neutrons in shell model orbitals calculated in single particle potentials constrained to reproduce the above mentioned rms radii and reproducing also the experimental binding energies for the $1d_{3/2}$ protons and neutrons. Although the parameters of the effective interaction resulting from the different matter density distributions assumed for $^{40}$Ca were rather different[4] no significant changes were observed in the results obtained for the heavier Ca isotopes when one distribution for $^{40}$Ca was replaced by the other, provided the FB method was used in the folding model (see sect. III).

The final empirical effective interaction used for most of the analyses discussed below is displayed in fig. 3 a for a free nucleon ($r_N = \infty$) and for nucleons imbedded in a $^{40}$Ca nucleus at different radii $r_N$ characterizing the saturation effect. This interaction was determined assuming a 3-parameter Fermi form for the nucleon density distribution with the parameter values for protons given above and for neutrons given by $c_n = 3.748$ fm, $a_n = a_p$, $w_n = w_p$. The interaction parameter values determined from the fit to $^{40}$Ca are $V_G = 64.6 \pm 0.5$ MeV, $a = 1.798 \pm 0.002$ fm and $\gamma = 1.9 \pm 0.1$ fm$^2$. It is interesting to note that the phenomenological value for $\gamma$ is very close to 2 fm$^2$ as found in more fundamental investigations[26].

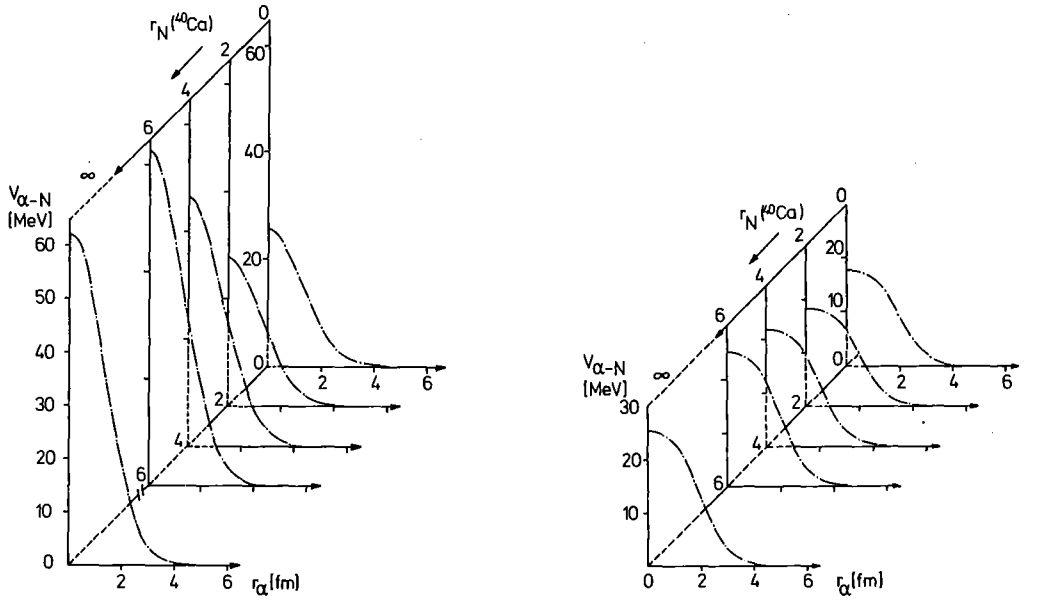


Fig. 3a) Effective phenomenological N-α-interaction respecting saturation effects due to the target nucleus density for scattering of 104 MeV alpha-particles from $^{40}Ca$.

3b) Microscopic interaction[6,9].

The phenomenological Gaussian N-α-interaction can be compared with a microscopic interaction generated from Green's density dependent effective nucleon-nucleon interaction including antisymmetrization effects[6,9] as shown in fig. 3b. Only the strength and the saturation factor $\gamma$ have been adjusted to the $^{40}Ca(\alpha,\alpha)$ cross sections. A good agreement is observed for $r_\alpha \gtrsim 2$ fm and $r_N \gtrsim 2$ fm indicating that the interaction is well understood except of the very interior region of the nucleus. The description of the cross sections by the microscopic interaction is only slightly worse when compared to the phenomenological Gaussian interaction. The results concerning the differences of the four Ca-isotopes are consistent when using the phenomenological or microscopic interaction, respectively. Hence, details of the interaction seem to be less important than consistent application of the folding model where it is certainly important to regard only a restricted range of target mass numbers.

The theoretical angular distribution calculated with the quoted parameter values of $\rho_m$ and the effective interaction shown in fig. 3a is displayed in fig. 5 (top). The importance of the saturation term is demonstrated in fig. 4 where we set $\gamma=0$. In this case the forward angular distribution (corresponding to grazing collisions in the low density region) is still rather well described whereas the large angle behavior is not at all reproduced by the theoretical curve.

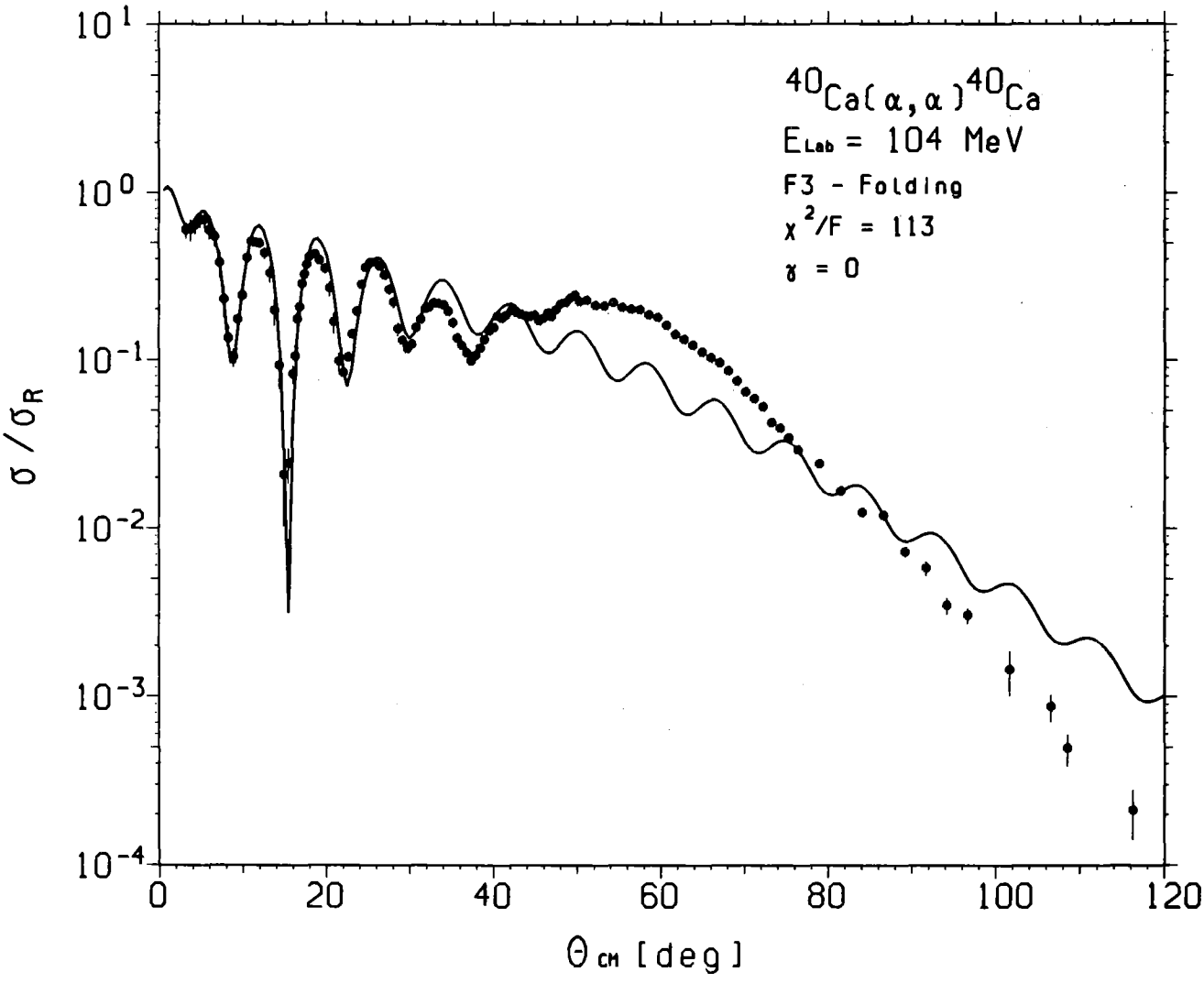


Fig. 4 Experimental and theoretical angular distribution of elastic alpha-particle scattering from $^{40}Ca$ using a folding model <u>without</u> saturation term (see eq. 3).

## 2.2 Nuclear Density Distributions

In the same way as described above the point-proton distributions of the other Ca-isotopes can be derived from the well-known experimental charge distributions by unfolding the proton charge form factor. Assuming additionally the neutron distributions to have the same form and rms-radius as the proton distributions we calculated the theoretical angular distributions of $^{42,44,48}$Ca using the folding model (eq. 3) and varying only the imaginary part of the optical potential. The results shown in fig. 5 are characterized by a poor reproduction of the positions of the oscillation minima (in particular for $^{48}$Ca). Also the slope of the angular distributions at large angles is poorly described by this procedure.

The failure of the density dependent folding model in the case of the heavier Ca-isotopes can in principle either be due to

(i) a significant change of the effective interaction, when going from $^{40}$Ca to the heavier isotopes or

(ii) a violation of the assumption $\langle r_n^2 \rangle^{1/2} = \langle r_p^2 \rangle^{1/2}$.

Investigations based on pure microscopic calculations including density dependence and exchange effects showed[13], however, that even by drastic changes of the density dependence of the interaction one cannot generate a reasonable optical potential (which is well known from the FB-potential analyses[3]) without additionally assuming the neutron density to be different from the proton density at least for $^{48}$Ca. Therefore, we assumed the effective interaction to be constant over the mass number range of the Ca-isotopes and extracted the matter densities by varying the parameters of $\rho_m$. Table Ia summarizes results obtained by using a 3-parameter Fermi form. The corresponding experimental and theoretical differential cross sections are shown in fig. 6.

The imaginary potential was a conventional Saxon-Woods (SW) one. The values of $\chi^2/F$ should be compared with those obtained from optical model fits using the FB description of the real potential[3] because those may serve as estimates of the best values attainable using an optical

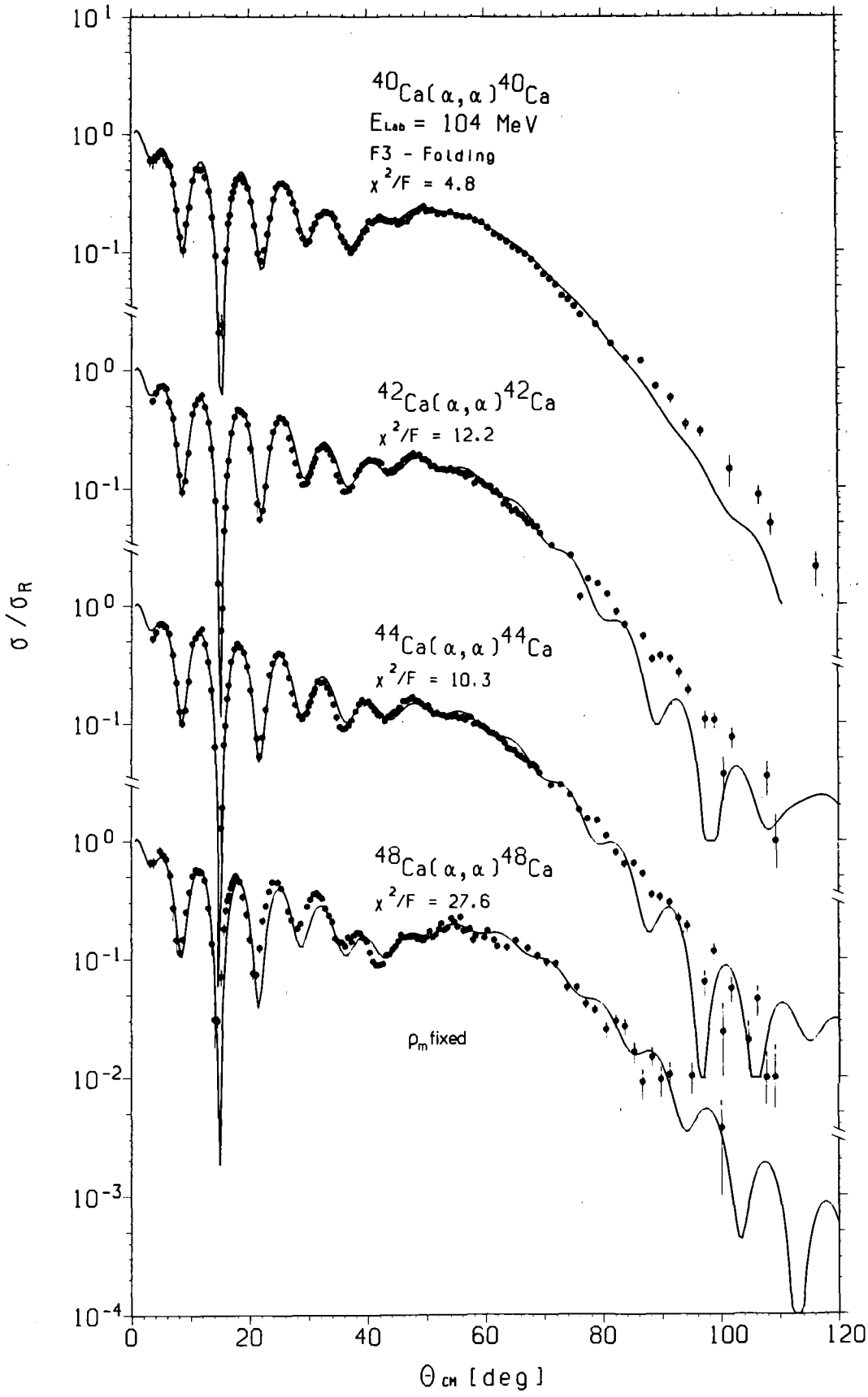


Fig. 5 Differential elastic scattering cross sections (divided by the Rutherford cross sections) and folding model descriptions with fixed matter densities assuming $\langle r^2 \rangle_n^{1/2} = \langle r^2 \rangle_p^{1/2}$.

model with SW form for the imaginary potential. It is evident that although reasonable fits are obtained the constraints imposed by the folding model lead to larger values of $\chi^2/F$. The values of $-J_v/4A$ and $\langle r^2_{pot}\rangle$, the volume integral of the real potential per nucleon pair and its rms radius, do not agree precisely with those obtained from the FB potentials, presumably due to the added constraints in the folding model. However, they are much closer to the FB-potential values than are results of the folding model <u>without</u> the saturation term [9] and they reproduce the trend of the phenomenological values when comparing the different isotopes. The values of $\langle r^2_m\rangle^{1/2}$, the rms radius of the nuclear density distributions, show an increase with increasing number of neutrons. Values of $\langle r^2_p\rangle^{1/2}$, the rms radius for the proton distributions[10] are also included in the Table. In Table I(b) similar results are given for an effective interaction based on 2-parameter Fermi distributions for $^{40}$Ca as previously used[4].

TABLE I: Results for density dependent folding model

| Target | $\chi 2/F$ | $-J_v/4A$ (MeV fm$^3$) | $\langle r^2_{pot}\rangle^{1/2}$ (fm) | $\langle r^2_m\rangle^{1/2}$ (fm) | $\langle r^2_p\rangle^{1/2}$ * (fm) |
|---|---|---|---|---|---|
| | | (a) 3-parameter Fermi for $^{40}$Ca realistic double folded coulomb potential from experimental charge distributions | | | |
| $^{40}$Ca | 4.8 | 309.4 | 4.253 | 3.367 | 3.386 |
| $^{42}$Ca | 4.9 | 299.6 | 4.261 | 3.336 | 3.422 |
| $^{44}$Ca | 4.9 | 300.0 | 4.311 | 3.399 | 3.439 |
| $^{48}$Ca | 3.6 | 311.0 | 4.396 | 3.589 | 3.409 |
| | | (b) 2-parameter Fermi for $^{40}$Ca** Coulomb potential from charged sphere | | | |
| $^{40}$Ca | 4.7 | 310.4 | 4.275 | 3.367 | 3.386 |
| $^{42}$Ca | 6.4 | 304.9 | 4.348 | 3.395 | 3.422 |
| $^{44}$Ca | 5.4 | 302.1 | 4.363 | 3.423 | 3.439 |
| $^{48}$Ca | 5.5 | 309.6 | 4.394 | 3.544 | 3.409 |

* Ref. 10 ** Ref. 4

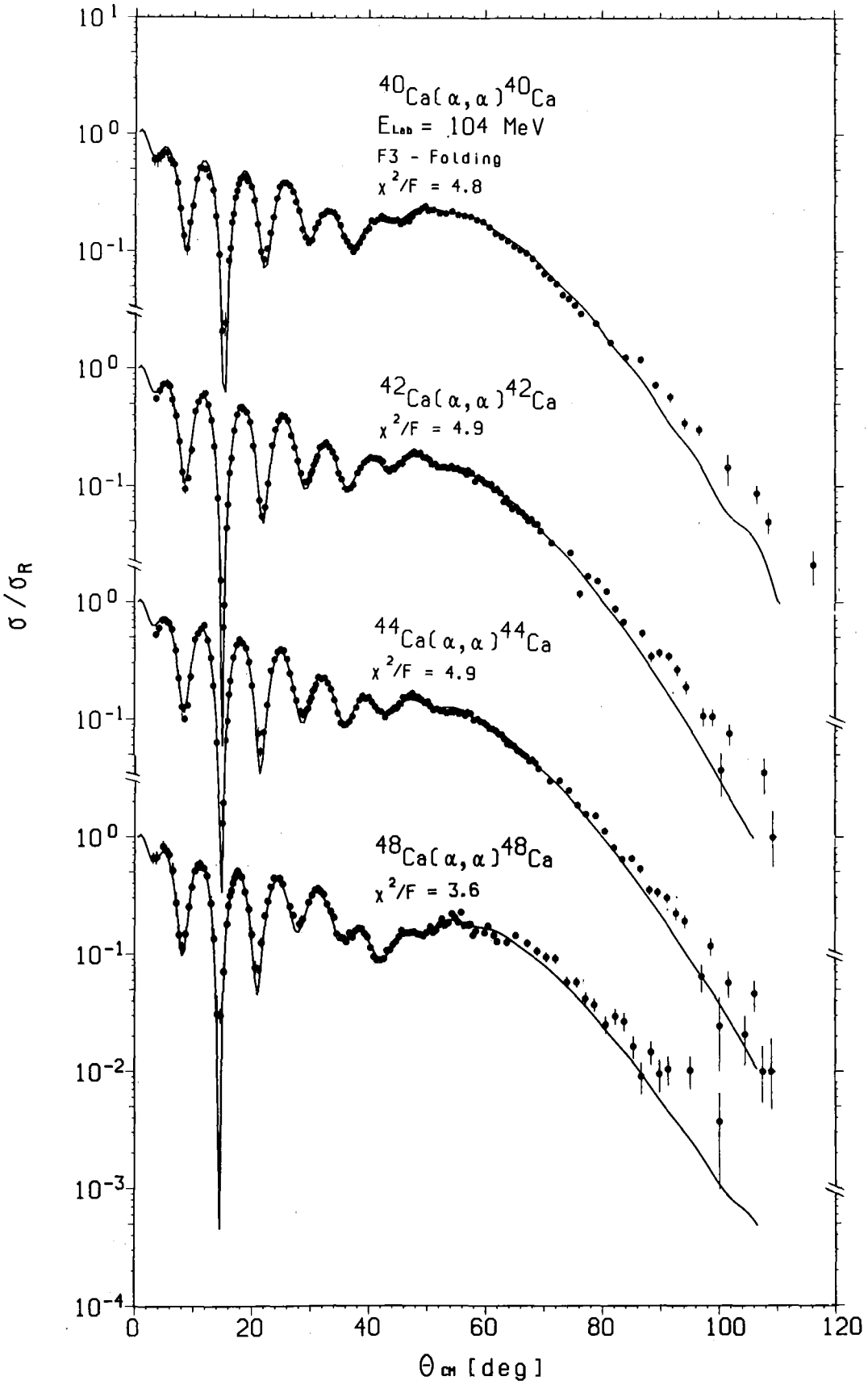


Fig. 6 Differential cross sections of elastic scattering normalized to the Rutherford scattering cross sections and density dependent folding model description using matter densities with 3-parameter Fermi-form (F3).

Comparing the two sets of results one notes the undesirable dependence on the choice of parameters or choice of functions and of particular procedures (e.g. the treatment of the Coulomb potential) and therefore the need for some improvement is quite obvious. Another difficulty with the above results is that there is no simple way of estimating the uncertainty of the various quantities. Both problems are dealt with in the following section.

## 3. FOURIER-BESSEL FOLDING MODEL

This modification to the folding model is a natural extension which significantly reduces the dependence of the results on the choice of a particular type of analytic function for the various densities. The added flexibility is also expected to improve the fits to the data.

In the FB folding model[4] one uses the effective interaction given by eq. (3) with parameters determined from fits to the $^{40}Ca$ data but replacing $\rho_m$ by the following expression:

$$\rho_m(r) = \rho_o(r) + \sum_{n=1}^{N'} \beta_n \, j_o \left(\frac{n\pi r}{R'_c}\right) \tag{5}$$

where $\rho_o(r)$ is a suitably chosen function normalized to have a volume integral of A, the mass number of the target. For $r > R'_c$ only $\rho_o$ is retained. With this choice, the second term in (5) must have a vanishing volume integral and that is achieved by imposing the constraint

$$\beta_1 = \sum_{n=2}^{N'} \frac{(-1)^n \beta_n}{n^2} \tag{6}$$

In the $\chi^2$ fit to the data the parameters $\beta_2 \ldots \beta_{N'}$ are varied together with the SW imaginary potential. The number of terms N' and the value of the cut-off radius $R'_c$ are usually smaller than the corresponding values in the FB potential fits[3,9]. The function $\rho_o$ may be conveniently chosen as $A/Z \cdot \rho_p$, with Z the charge number of the target and $\rho_p$ the density distribution of the protons or it may be taken from the results of section II (Table I). However, different choices of $\rho_o$ lead to very similar converged results[9]. Uncertainties are calculated as in Ref. 4 (note that all

expressions for uncertainties in Ref. 4 should be multiplied by $\sqrt{2})^3$.

The experimental data have been described with the density dependent folding model (3) varying the coefficients of the FB densities (5) in $\chi^2$ fit procedures. Different combinations of interaction parameters were used as determined from the different models assumed for the density of $^{40}$Ca (see section II). In particular, full consistency was observed when varying also FB-coefficients for $^{40}$Ca. The density distributions thereby obtained agreed, within the uncertainties, with those initially assumed for $^{40}$Ca and which served as the basis for the parameters of the effective interaction. Table II(a) summarizes the results obtained from several fits where values of $R'_c$ and $N'$ were varied over reasonably wide ranges. Comparisons between experimental cross sections and fits based on FB-densities are displayed in Fig. 7. In Ref. 4 we explored the effects of adjusting $V_G$ also for isotopes other than $^{40}$Ca. Doing so in the present analysis did not produce any systematic effects[9] and the results were consistent with the average values given in Table II(a).

We have also investigated the $^{48}$Ca case taking into account some of the additional information available for this nucleus. Thereby, for the protons a density distribution was calculated from single particle potential and $\rho_n$, the neutron density distribution, was split into $\rho_n=\rho_{nc}+\rho_{ex}$ , the sum of the "neutron core" of Z neutrons and of the (N-Z) excess neutrons. $\rho_{ex}$ was calculated from a single particle potential reproducing the binding energy and the rms radius[11] as determined from nucleon transfer reactions. $\rho_{nc}$ was represented in terms of a 3-parameter Fermi function the parameters of which were determined from a fit to the $^{48}$Ca data. A good fit to the data was obtained and the resulting rms radii agreed with those given in Table II. It is therefore concluded that no specific shell effects are observed in the $^{48}$Ca data.

Fig. 8 presents the density distributions obtained from the FB folding procedure and in Fig. 9 the differences between the density distributions

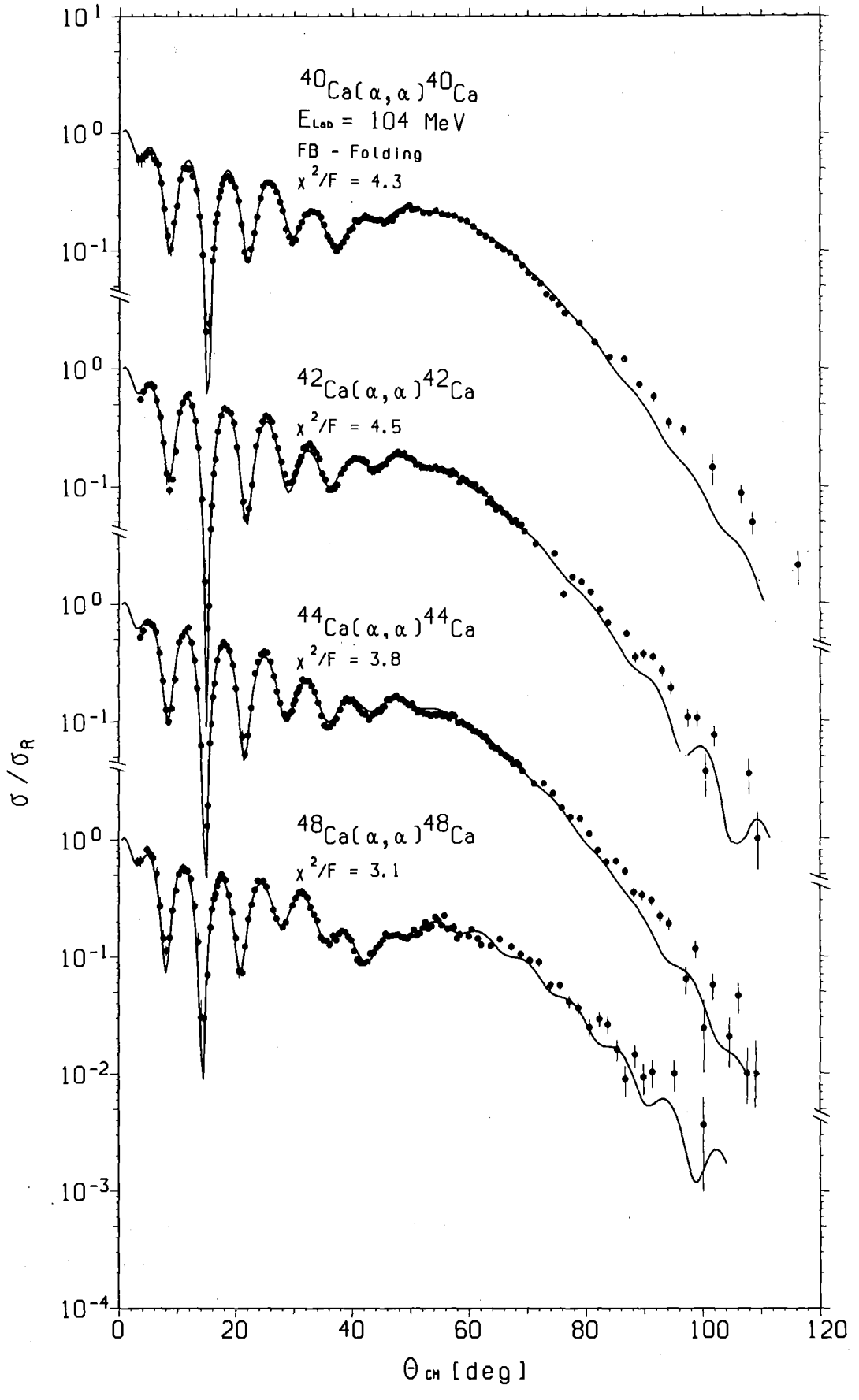


Fig. 7 Ratios of elastic scattering cross sections to Rutherford cross sections: comparisons between experiment and best fit FB folding model.

TABLE II(a): Results for FB density dependent folding model

| Target | $\chi^2/F$ | $-J_v(4A)$ (MeV fm$^3$) | $\langle r^2_{pot}\rangle^{1/2}$ (fm) | $\langle r^2_m\rangle^{1/2}$ (fm) |
|---|---|---|---|---|
| $^{40}$Ca | 4.3 | 310.0 | 4.262 | 3.36 ± 0.03 |
| $^{42}$Ca | 4.5 | 303.9 | 4.292 | 3.42 ± 0.03 |
| $^{44}$Ca | 3.8 | 303.7 | 4.330 | 3.46 ± 0.03 |
| $^{48}$Ca | 3.1 | 309.2 | 4.391 | 3.54 ± 0.04 |

TABLE II(b): Integral quantities of FB potentials (from Ref. 3)

| | | | |
|---|---|---|---|
| $^{40}$Ca | 2.0 | 327 ± 3 | 4.37 ± 0.06 |
| $^{42}$Ca | 2.5 | 317 ± 3 | 4.38 ± 0.06 |
| $^{44}$Ca | 2.7 | 314 ± 3 | 4.41 ± 0.07 |
| $^{48}$Ca | 2.3 | 319 ± 5 | 4.49 ± 0.09 |

of $^{42,44,48}$Ca and $^{40}$Ca are displayed. The differences $\Delta\rho_m$ have been multiplied by $4\pi r^2$, as is customarily done in the analysis of electron scattering[12]. Note, however, that the densities are not determined at all at small radii, and the multiplication by $r^2$ serves only to emphasize the region where the differences are well-determined.

## 4. COMPARISONS WITH THE FB POTENTIAL

The results of the FB folding procedure given in Table II could be compared with the results of the FB potential procedure presented in Table II of Ref.3. For convenience, the results of Ref. 3 are included in Table II(b). One may wish to use the results of the FB potential analysis to perform an "unfolding" interpretation of the rms radii of the potentials

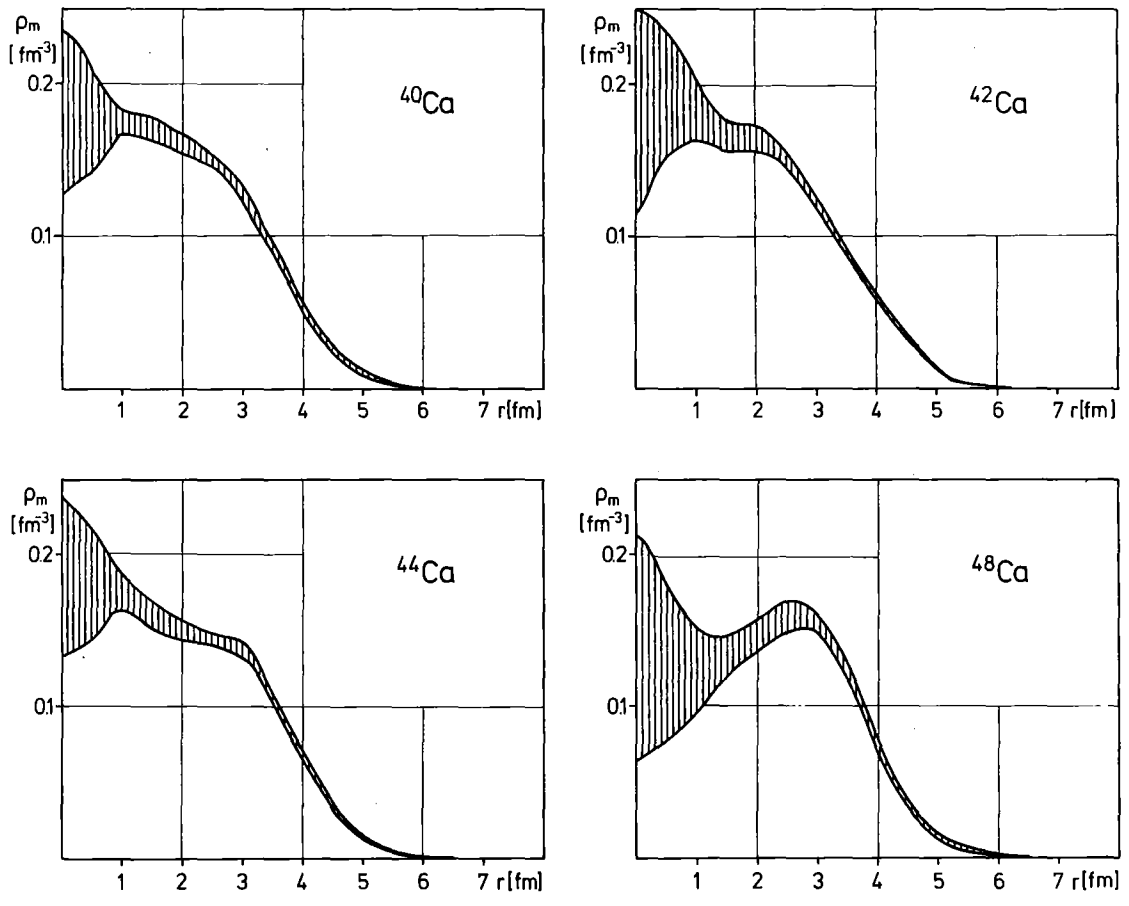


Fig. 8: Nuclear densities of $^{40,42,44,48}Ca$ obtained from analyses using Fourier-Bessel densities. The hatched areas indicate the error band.

$\langle r^2_{pot} \rangle^{1/2}$. The simple density-independent folding model (1) requires the volume integrals per nucleon pair $-J_v/4A$ to be equal for different isotopes and the difference between the mean square potential radii $\langle r^2_{pot} \rangle$ of two isotopes to be equal to the corresponding difference between the mean square matter radii $\langle r^2_m \rangle$

$$\Delta\langle r^2_{pot} \rangle = \Delta\langle r^2_m \rangle. \qquad (6)$$

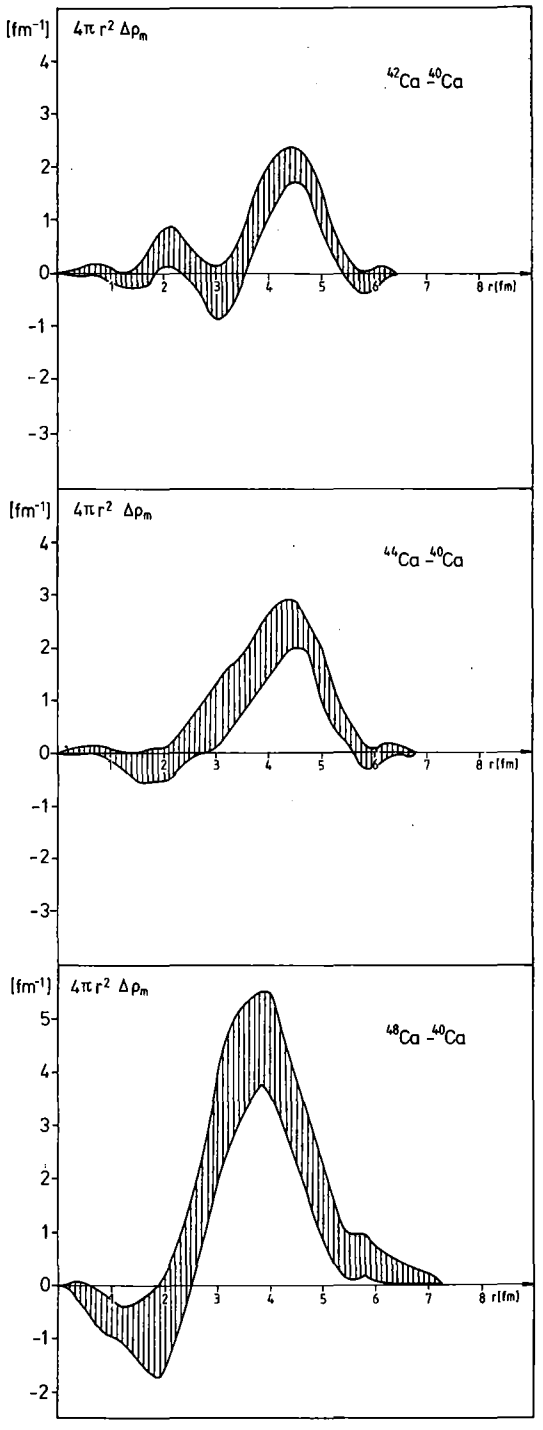


Fig. 9 Differences of the nuclear densities $4\pi r^2(\rho_m(A) - \rho_m(40))$ from various density dependent folding model analyses using Fourier-Bessel densities. The hatched areas indicate the error band.

Due to the density dependence in the folding model these relationships do not necessarily hold and indeed the observed values of $-J_v/4A$ are not exactly the same for all targets in the FB potential method as well as in the FB folding analyses. However, evaluating the differences

$$\delta^2 = \langle r^2_{pot} \rangle - \langle r^2_m \rangle \qquad (7)$$

from the FB density dependent folding results (Table IIa, columns 4 and 5) a rather constant value for $\delta^2$ is obtained for the four isotopes. This suggests that the density dependence of the interaction modifies less the additivity of ms radii than the constancy of $-J_v/4A$. Fully microscopic double folding calculations[13] support this conclusion. One may therefore use values of $\langle r^2_{pot} \rangle^{1/2}$ to study differences between $\langle r^2_m \rangle^{1/2}$, at least over an isotopic sequence.

However, it is not clear at all that the differences between values of $\langle r^2_m \rangle^{1/2}$ are the relevant presentation of the differences between $\rho_m$ of the various isotopes, as extracted from experiments of alpha particle scattering. The functions $\Delta\rho_m$ displayed in Fig. 9 may be the more appropriate presentation of the information provided by the experiment.

## 5. COMPARISONS WITH OTHER METHODS

The elastic scattering of protons[14-16], of α particles[17-19], and of pions[20,21], total cross section measurements for protons[22] and pions[23] and observations of pionic atoms[23,24] have all been used for studies of the nuclear density distributions of calcium isotopes. Table III summarizes values of $\langle r^2_m \rangle^{1/2}(A) - \langle r^2_m \rangle^{1/2}(40)$ obtained from the various methods. Comparing the present results with those obtained from other experiments of elastic scattering of α particles we note that the flexible ("model independent") FB method had not been applied before for Ca-nuclei except $^{40}Ca$ [16] so that previous results are not free from systematic errors arising from specific assumptions about the form of the distributions. In particular, when only the diffraction region is included in the analysis, the nuclear interior is not probed and the density distribution in the

interior is essentially postulated through the chosen function for the density distribution. All previous experiments of alpha particle scattering around 100 MeV were confined to the diffraction region of the angular distribution. Indeed, if we analyze only the diffraction part of our data we find values of $\langle r_m^2 \rangle^{1/2}$ quite different from those quoted for the full data, strongly depending on the assumptions made on the density.

The analysis of 1 GeV proton scattering[14-16] is a promising method thanks to the plausibility of using the free p-nucleon interaction in constructing the p-nucleus interaction. Methods like the FB one have already been used[16] for the analysis. However, the reaction models are unable to reproduce the experimental data at angles beyond the third diffraction minimum and analyses have therefore been confined to very forward angles. This presumably leads to similar consequences regarding the nuclear interior as discussed above. In contrast, in the present work

TABLE III. Values of $\langle r_m^2(A) \rangle^{1/2} - \langle r_m^2(40) \rangle^{1/2}$ (in fm) obtained by different methods

| Method | 42 | 44 | 48 | ref. |
|---|---|---|---|---|
| present | 0.06 ± 0.03 | 0.10 ± 0.03 | 0.18 ± 0.04 | |
| 1 GeV proton scattering | 0.055± 0.02 | 0.07 ± 0.02 | 0.10 ± 0.02 | 14 |
| 8oo MeV pol.prot.scat. | 0.08 ± 0.08 | 0.08 ± 0.08 | 0.09 ± 0.08 | 15 |
| 6oo MeV and 1 GeV proton (FB) | 0.04 ± 0.04 | 0.08 ± 0.04 | o.13 ± 0.04 | 16 |
| 1.37 GeV α-scattering | 0.06 ± 0.03 | 0.09 ± 0.03 | 0.12 ± 0.03 | 17 |
| 166 MeV α-scattering | - | 0.11 ± 0.16 | 0.22 ± 0.12 | 18 |
| 79 MeV α-scattering | - | - | 0.05 ± 0.04 | 19 |
| p total cross sect. | - | 0.05 ± 0.09 | 0.36 ± 0.09 | 22 |
| $\pi^+$ cross sect. | - | 0.06 ± 0.07 | 0.09 ± 0.07 | 23* |
| pionic atoms | - | 0.05 ± 0.05 | 0.09 ± 0.05 | 24,25 |

* taking $\Delta\langle r_p^2 \rangle^{1/2}$ from Ref. 10

the density dependence was introduced into the folding model for α particle scattering in order to be able to extend the analyses over the full range of angles that had been measured.

The elastic scattering of pions was analyzed[20,21] using a simplified model (of a black disc) and the results so obtained could strongly depend on those assumptions. Total cross sections[22,23] and pionic atoms[24,25] provide only one or two experimental numbers (cross sections or level shift and width) and therefore the analysis must rely on the choice of functions for the density distributions. It is therefore not clear whether the results of these experiments can be presented by rms radii particularly when looking for small isotopic differences. In view of the above arguments one should also ask the question whether all the other experiments (if any) really determine the rms radii of the nuclear density distribution. Some of the conflicts between different results as observed in Table III may be resolved if a combined analysis is made of several experiments which probe different radial regions of the nucleus. For example, it is possible that moments of the density distributions different from the second are better determined[16] by some experiments and analyses of different moments may prove useful. Calculating several radial moments of the real potentials and of the nuclear density distributions for the various isotopes, as determined from the present experiment, shows that the $2^{nd}$, $3^{rd}$ and $4^{th}$ moments ($\langle r^2\rangle^{1/3}$, $\langle r^3\rangle^{1/3}$ and $\langle r^4\rangle^{1/4}$) are equally well determined. The isotopic differences observed in the $3^{rd}$ and $4^{th}$ moments are very similar to those observed in the rms radius.

We wish to thank Mrs. Orna Millo of the Racah Institute for help with the calculations.

1 H. Rebel, in: Radial shape of nuclei, eds. A. Budzanowski and A. Kapuscik (Cracow, 1976) p. 164.

2 D.A. Goldberg and S.M. Smith; Phys. Rev. Lett. 29, 500 (1972).

3 H.J. Gils, E. Friedman, H. Rebel, J. Buschmann, S. Zagromski, H. Klewe-Nebenius, B. Neumann, R. Pesl and G. Bechtold; Report KfK 2838, Karlsruhe (1979).

4 E. Friedman, H.J. Gils, H. Rebel, and Z. Majka, Phys. Rev. Lett. 41, 1220 (1978).

5 D.F. Jackson and V.K. Kembhavi; Phys. Rev. 178, 1626 (1969)
A.M. Bernstein, Advances in Nucl. Phys. eds.
M. Baranger and E. Vogt (Plenum Press, New York, 1969)
H. Rebel, in: Proc. Int. School on Nucl. Phys. ed. A. Ciocanel (Predeal, Romania 1974).

6 Z. Majka, H.J. Gils, and H. Rebel; Z. Physik A288, 139 (1978)

7 E. Friedman and C.J. Batty; Phys. Rev. C 17, 34 (1978).

8 J.W. Negele; Phys. Rev. C 1, 1260 (1970)
J.W. Negele and D. Vautherin; Phys. Rev. C 5, 1472 (1970)
X. Campi and D. Sprung; Nucl. Phys. A194, 401 (1972).

9 H.J. Gils; in Proc. Int. Discussion Meeting "What Do We Know about the Radial Shape of Nuclei in the Ca-Region?" (Karlsruhe, 2-4 May 1979) Report KfK 2830.

10 H.D. Wohlfahrt, E.B. Shera, M.V. Hoehn, Y. Yamazaki, G. Fricke, and R.M. Steffen, Phys. Lett. 73B, 131 (1978).

11 E. Friedman, A. Moalem, D. Suraqui and S. Mordechai; Phys. Rev. C 14, 2082 (1976).

12 H.D. Wohlfahrt, D. Schwentker, G. Fricke, H.G. Andresen, E.B. Shera, G.A. Rinker, R.B. Perkins, E.T. Ritter, L. Wagner, R.M. Steffen; Contr. paper at Radial shape of nuclei (Cracow, 1976).
H.D. Wohlfahrt; Proc. Int. Discussion Meeting "What do we know about the radial shape of Nuclei in the Ca-Region?" (Karlsruhe, (2-4 May 1979) Report KfK 2830.

13 Z. Majka, Phys. Lett. 76B, 161 (1978).
Z. Majka, H.J. Gils, and H. Rebel, to be published
Proc. Int. Discussion Meeting "What do we Know about the Radial Shape of Nuclei in the Ca-Region?" (Karlsruhe 2-4 May, 1979), Report KfK 2830.

14 S. Shlomo and R. Schaeffer; Phys. Lett. 83B, 5 (1979).

15 G. Igo, G.S. Adams, T.S. Bauer, G. Pauletta, C.A. Whitten, Jr., A. Wreikat, G.W. Hofmann, G.S. Blanpied, W.R. Coker, C. Harvey, R.P. Liljestrand, L. Ray, J.E. Spencer, H.A. Thiessen, C. Glashausser, N.M. Hintz, M.A. Oothoudt, H. Nann, K.K. Seth, B.E. Wood, D.K. McDaniels, and M. Gazzaly; Phys. Lett. 81B, 151 (1979).

16 I. Brissaud and M.K. Brussel; J. Phys. G. (Nucl. Phys. ) 3, 481 (1977).
I. Brissaud and X. Campi; Phys. Rev. C 15, 452 (1977).
Proc. Int. Discussion Meeting "What do we Know about the Radial Shape of Nuclei in the Ca-Region?" (Karlsruhe 2-4 May, 1979) Report KfK 2830.

17 G.D. Alkhazov, T. Bauer, R. Bertini, L. Bimbot, O. Bing. A. Boudard, G. Bruge, H. Catz, A. Chaumeaux, P. Couvert, J.M. Fontaine, F. Hibou, G.J. Igo, J.C. Lugol, and M. Matoba; Nucl. Phys. A280, 365 (1977).

18 I. Brissaud, Y. Le Bornec, B. Tatischeff, L. Bimbot, M.K. Brussel, and G. Duhamel; Nucl. Phys. A191, 145 (1972).

19 G.M. Lerner, J.C. Hiebert, L.L. Rutledge, Jr., C. Papanicolas, and A.M. Bernstein; Phys. Rev. C 12, 778 (1978).

20 J.-P. Egger, R. Corfu, P. Gretillat, C. Lunke, J. Piffaretti, E. Schwarz, C. Perrin, J. Jansen, and B.M. Preedom; Phys. Rev. Lett. 39, 1608 (1977).

21 M.B. Johnson and H A. Bethe; Comments Nucl. and Part. Physics 8, 75 (1978).

22 B.D. Anderson, P.R. Bevington, F.H. Dverna, M.W. McNaughton, H.B. Willard, R.J. Barrett, N.S.P. King, and D.J. Ernst; Phys. Rev. C 19, 905 (1979).

23 M.J. Jakobson, G.R. Burleson, J.R. Calarco, M.D. Cooper, D.C. Hagerman, I. Halpern, R.H. Jeppeson, K.F. Johnson, L.D. Knutson, R.E. Marrs, H.O. Meyer, and R.P. Redwine, Phys. Rev. Lett. 38, 1201 (1977).

24 C.J. Batty, S.F. Biagi, E. Friedman, S.D. Hoath, J.D. Davies, G.J. Pyle, G.T.A. Squier, D.M. Asbury, and M. Leon; Phys. Lett. 81B, 165 (1979).

25 E. Friedman; Analysis of preliminary results from Los Alamos, H.D. Wohlfahrt, private communication.

26 J.P. Jeukenne, A. Lejeune, and C. Mahaux; Phys. Rev. C16, 80 (1977).